Energetics of Codon−Anticodon Recognition on the Small Ribosomal Subunit†

Martin Almlöf, Martin Andér, and Johan Åqvist*

Department of Cell and Molecular Biology, Uppsala University Biomedical Center, Box 596, SE-751 24 Uppsala, Sweden

Received August 22, 2006; Revised Manuscript Received November 1, 2006

ABSTRACT: Recent crystal structures of the small ribosomal subunit have made it possible to examine the detailed energetics of codon recognition on the ribosome by computational methods. The binding of cognate and near-cognate anticodon stem loops to the ribosome decoding center, with mRNA containing the Phe UUU and UUC codons, are analyzed here using explicit solvent molecular dynamics simulations together with the linear interaction energy (LIE) method. The calculated binding free energies are in excellent agreement with experimental binding constants and reproduce the relative effects of mismatches in the first and second codon position versus a mismatch at the wobble position. The simulations further predict that the Leu2 anticodon stem loop is about 10 times more stable than the Ser stem loop in complex with the Phe UUU codon. It is also found that the ribosome significantly enhances the intrinsic stability differences of codon−anticodon complexes in aqueous solution. Structural analysis of the simulations confirms the previously suggested importance of the universally conserved nucleotides A1492, A1493, and G530 in the decoding process.

The ribosome is an impressive machinery that accomplishes the translation of the genetic code into working proteins. In order to sustain cell growth, the ribosome must be able to perform its task at a high enough rate, without sacrificing fidelity. Ribosome fidelity starts at the aminoacyl-tRNA (aa-tRNA)[1] selection stage where EF-Tu·GTP·aa-tRNA is accommodated into the A-site of the 30S subunit. Selection is based on correct Watson−Crick base complementarity between the anticodon of aa-tRNA and the codon of mRNA already in the A-site. Studies have shown that the frequency of incorporating erroneous amino acids into the growing peptide chain during protein synthesis is of the order 10^{-4} (*1*). A direct translation of this error frequency into binding energy would require an average difference in the free energy of binding between correct and incorrect aa-tRNAs of about 7 kcal/mol at 300 K. However, the observed free energy difference for base pairing in solution is not sufficient to account for the level of specificity shown in the protein synthesis, especially not in discriminating between cognate and so-called near-cognate aa-tRNAs, which differ only by a single mismatch. For example, the observed free energy difference of helix formation upon changing an A-U base pair to a G-U mismatch is about 0−3 kcal/mol (*2*, *3*). Several mechanisms have been suggested to explain this (*4*−*7*), and among them the concept of proofreading (*6*, *7*), where the base pairing is evaluated in two steps separated by an irreversible step of GTP hydrolysis, was subsequently verified experimentally (*8*, *9*).

In theory, the energetics of codon matching can be utilized both in initial selection and in proofreading, and the difference in base-pairing interactions alone between cognate and near-cognate codon−anticodon complexes could then be able to achieve the observed specificity, if exploited twice and separated by an irreversible step. However, more recent findings suggest that this view is too simplistic (*10*−*15*). There is compelling evidence that G530, A1492, and A1493 of 16S rRNA interact with the minor groove of the codon−anticodon complex, in a manner that is specific to correct Watson−Crick geometry but independent of sequence (*14*, *15*). Thus, in addition to the interactions between codon and anticodon, the ribosomal decoding center is proposed to discriminate against incorrect aa-tRNA based on interactions between the aa-tRNA and mRNA and the ribosome itself. This means that the internal selectivity of codon recognition is enhanced by a stereospecific component provided by the ribosome.

It has also been suggested that the stability of the codon−anticodon complex is not used for aa-tRNA selection but that this process is entirely kinetically controlled (*16*). That is, Gromadski and Rodnina (*16*) reported a 350-fold difference in dissociation rates between cognate and near-cognate complexes, but this rate does not affect k_{cat}/K_M for cognate substrate since codon recognition rather than subsequent GTP hydrolysis is rate-limiting in this case. For near-cognate substrates, on the other hand, GTP hydrolysis instead becomes rate-limiting and is 650 times slower than for correct aa-tRNA (*16*). Hence, while the initial selection may be viewed as kinetically controlled, it is still the case that a slower near-cognate dissociation rate (more stable codon recognition complex) would increase k_{cat}/K_M for near-cognate substrates and therefore reduce the initial selection factor. The binding of incorrect substrate probably also has an indirect effect on k_{cat} itself through a nonoptimal positioning

† Support from the Swedish Research Council (VR) is gratefully acknowledged.

* Corresponding author. Phone: +46 18 471 4109. Fax: +46 18 53 69 71. E-mail: aqvist@xray.bmc.uu.se.

[1] Abbreviations: MD, molecular dynamics; aa-tRNA, aminoacyl tRNA; ASL, anticodon stem loop; rms, root mean square; RMSF, root mean square fluctuations; RDF, radial distribution function.

10.1021/bi061713i CCC: $37.00
Published on Web 01/02/2007

of the EF-Tu·GTP·aa-tRNA complex for GTPase activation and GTP hydrolysis.

In view of the importance for the ribosome to be able to discriminate against incorrect substrates, it is thus of considerable interest to evaluate the detailed energetics of codon−anticodon recognition utilizing atomic resolution 3D structures, which has not been done before. While initial tRNA selection in the decoding process is more complex and also depends on other interactions, e.g., involving EF-Tu, the energetics of codon−anticodon interactions is of fundamental interest since codon matching is at the heart of specificity. Furthermore, the available experimental energetics of anticodon stem loop binding to the decoding center (*15*) provides an unequivocal benchmark for computational analysis, allowing a more direct comparison than the measured kinetics of initial selection. The energetic complexity of intact tRNA binding to the ribosome is, for example, illustrated in recent studies by Uhlenbeck and co-workers (*17*, *18*), who found that posttranscriptional tRNA modifications can offset the differential binding of the amino acid and anticodon parts, rendering a uniform binding of cognate aa-tRNAs to the ribosome. It was also shown that intramolecular tRNA base pairs close to the anticodon loop can modulate binding to the ribosome (*18*). The fact that tRNAs have evolved to achieve a more or less uniform binding to their cognate mRNAs indeed suggests that cognate vs noncognate discrimination is largely determined by codon−anticodon interactions, both through direct binding affinities and through structural positioning required for the GTPase and peptidyl transferase activities.

Computer simulations of the process of codon recognition on the ribosome have been made possible by the publishing of several crystal structures of the small ribosomal subunit (*15*, *19*). Sanbonmatsu and Joseph have earlier carried out a geometric analysis of codon−anticodon interactions on the ribosome using molecular dynamics (MD) calculations (*20*), in which they examined the dynamical fluctuations and structures of different codons in complex with the Phe-anticodon stem loop. These authors interestingly suggested a possible role of the mRNA kink, situated between the ribosomal A- and P-sites, in amplifying stability differences. While this hypothesis is intriguing, it is, however, very difficult to draw quantitative conclusions without calculating the actual energetics, since positional fluctuations cannot directly provide free energies. Herein we report a computational analysis of codon recognition together with calculated binding free energies, using the linear interaction energy method (LIE) (*21*) in combination with MD simulations, for near-cognate and cognate anticodon stem loops. The computer simulation results are found to be in very good agreement both with observed binding free energies and with structures and provide new predictions for those cases where experimental data do not exist. As is often the case with biomolecular systems, energetics appears also here as the most important link in structure−function correlation.

MATERIALS AND METHODS

All MD simulations were carried out using the program Q (*22*) with the CHARMM22 force field (*23*), as was the case also with earlier simulations of the peptidyl transfer reaction (*24*, *25*). The initial coordinates of the ribosome−tRNA complex were obtained from the crystallographic coordinates of the 30S ribosomal subunit [PDB accession code 1IBM (*15*)]. To correctly reflect the anticodon stem loop (ASL) present in the experimental binding studies, the ASL present in 1IBM was extended by aligning mutual residues in a fragment of yeast tRNA [PDB accession code 1EHZ (*26*)] with the ASL in 1IBM. P-site tRNA present in the experimental binding studies was modeled by aligning Cα's and phosphates in the ribosome-three-tRNA structure [including A-, P-, and E-site tRNAs, PDB accession code 1GIX (*27*)] with 1IBM. Starting structures for simulations which involved a near-cognate ASL bound in the A-site of the ribosome were generated with residue A1492 (*E. coli* numbering) modeled according to the near-cognate ribosome crystal structures with PDB accession codes 1N34 and 1N36. In these structures A1492 is not completely displaced out of the internal loop of helix 44 and thus does not span the codon−anticodon minor groove.

For both the free and bound ASL a 25 Å simulation sphere was centered on the N1 atom of the second nucleotide of the anticodon and thereafter solvated with CHARMM-modified TIP3P water (*23*). Any solute atoms outside the 25 Å sphere were tightly restrained throughout the entire simulation. Water molecules at the surface of the sphere were subjected to radial and polarization restraints to eliminate solvent boundary effects and reproduce experimental densities. In order to obtain a simulation sphere with zero net charge, Mg^{2+} ions were inserted at positions with high negative electrostatic potential as calculated with the Poisson−Boltzmann method using the APBS program (*28*). Residues with phosphates within 12.5 Å of the simulation center were modeled with a normal topology (i.e., with a net charge of −1 e), whereas residues with phosphates closer to the simulation sphere boundary were modeled with a charged or neutral topology depending on Mg^{2+} ion proximity. Prior to production phase MD, an 86 ps equilibration phase was performed. This equilibration consisted of stepwise heating from 10 to 300 K while heavy solute atoms were restrained to their initial positions by a harmonic potential [15−25 kcal/(mol·Å^2)]. During a 20 ps phase of the equilibration, hydrogen bonds between corresponding codon and anticodon bases were enforced using pairwise atom−atom distance restraints. The production phase consisted of 1 ns unrestrained MD. A 1 fs time step was used along with the SHAKE procedure (*29*) for all solvent bonds. Nonbonded interactions across the simulation sphere boundary were excluded. A nonbonded cutoff of 10 Å was used, with electrostatic interactions outside the cutoff approximated with the local reaction field multipole expansion (*30*). The ligand, which in the LIE framework (see below) consisted of the three bases of the anticodon, had no cutoff applied for its interactions. Nine replicate simulations of each ASL in bound and free states were carried out with randomized starting velocities from the Maxwell distribution.

Free energies of binding were calculated using the LIE method (*21*) from the energy differences between two simulations of each ASL, one in complex with the ribosome and one free in solution. In the present case we do attempt to calculate the absolute binding affinities of the entire ASLs but, in analogy with ref *31*, only evaluate the energetics

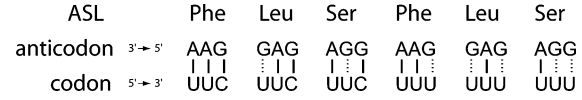

FIGURE 1: The different codon−anticodon interactions investigated by MD simulations in this work.

associated with the three anticodon bases. The binding free energy is then calculated from

$$\Delta G_{\text{bind}} = \alpha\Delta\langle V_{1-s}^{\text{vdW}}\rangle + \beta\Delta\langle V_{1-s}^{\text{el}}\rangle + \gamma \qquad (1)$$

Here the broken brackets are MD averages of the ligand-surrounding van der Waals or electrostatic energies and the Greek deltas denote the difference between these averages in the bound and free state. The electrostatic energies are scaled by a ligand-dependent parameter, β, which can take on a few different values in the range of 0.33−0.50 determined by a simple set of rules (*32*). In the present case the value of β is 0.43 for all of the bases in accordance with our earlier parametrization (*32*). The van der Waals energies are scaled by an empirically determined coefficient, α. In studies performed previously in our laboratory, an α of 0.18 has reproduced the binding free energies of various ligand−protein systems well, and it has been shown that α is neither system dependent nor force field dependent for the ligand−protein systems and force fields examined to date. γ is a constant term which may be required to reproduce absolute binding free energies, and it has been shown, in general, to reflect binding site hydrophobicity (*33*). Here, however, we follow the prescription from ref *31* and incorporate also the secondary interactions (excluding the three anticodon bases) into the constant γ. This has been shown to provide an efficient way of analyzing the energetics of point mutations at a larger interface (*31*).

RESULTS

In order to investigate the factors that discriminate between the binding of cognate and near-cognate tRNAs to the ribosome, simulations of three ASLs were performed in the free state (solvated in water) and complexed with solvated ribosome loaded with two different mRNAs with codon sequence UUC and UUU. The ASLs studied were the Phe ASL (ASL^{Phe}) with anticodon sequence 3′-AAG-5′, the Leu ASL (ASL^{Leu2}) with anticodon sequence 3′-GAG-5′, and the Ser ASL (ASL^{Ser}) with anticodon sequence 3′-AGG-5′ (Figure 1). These mRNAs and ASLs were chosen because binding data exist for them, and together they demonstrate cognate ASL binding as well as mismatches in the first (3′-GAG-5′ anticodon), second (3′-AGG-5′ anticodon), and third position (UUU codon) of the codon−anticodon helix. This allows us to investigate factors which determine discrimination of near-cognate vs cognate binding at each position of the codon−anticodon helix.

The initial structures of the simulations are all based on the 1IBM crystal structure, with minor modifications as described above. The only simulation that can be directly compared to 1IBM is that with ASL^{Phe} in the A-site and UUU as codon, since this represents the same mRNA−tRNA combination as that in the crystal structure. The average structure calculated from the nine replicate 1 ns simulations is shown in Figure 2, and it can immediately be seen that the agreement with the experimental structure is very good. An RMSD of 1.1 Å is obtained between the average MD structure and the 1IBM crystal structure for all atoms within 20 Å of the simulation sphere center.

The residue deviating the most from the crystal structure is C1054, which for all anticodon−codon combinations studied here shows a weak type of face-on stacking between the anticodon guanine in the third position (G34) and U1996, in contrast to the edge-on orientation observed in the crystal structure. Such a face-on and slightly more extended orientation enables C1054 to hydrogen bond to the nucleotide on the 3′ side of the codon and could perhaps help to maintain the reading frame (*34*).

Discrimination at the First Codon−Anticodon Base Pair. In the first position of the codon−anticodon helix, residue A1493 from the 16S RNA helix 44 closely monitors base pairing in an orientation known as a type I A-minor motif (*35*−*37*). The simulations clearly show that, irrespective of the base pairs studied here, both codon and anticodon nucleotides have strong interactions with A1493. In the simulations of ASL^{Phe} and ASL^{Ser}, where there is a Watson−Crick base pair in the first position, hydrogen bonds between the 2′-hydroxyl on A1493 and the codon 2′-hydroxyl, as well as between the anticodon 2′-hydroxyl and the N1 on A1493 ensure tight monitoring of the first base pair (Figure 3A,B). This pattern of interactions is sensitive to the geometry of the base pair in the first position and specifically favors Watson−Crick base pairs.

In the ASL^{Leu2} simulations, where the first position of the codon−anticodon helix is a G-U (wobble geometry) base pair, the type I A-minor motif pattern of interactions is lost. While the N2 atom on the first position guanine forms an additional hydrogen bond with N3 of A1493 compared to the cognate A-U case, the overall geometry of the first position base pair is altered in an unfavorable manner. In order to retain the wobble base-pairing geometry, the mRNA uracil in the first position is forced into an orientation where it loses its O2 hydrogen bond with A1493 (Figure 3C). As a result, the first position uracil is destabilized and fluctuates considerably throughout the ASL^{Leu2} simulations, whereas it is much more stable when base pairing to adenine. During the 1 ns production phase of the simulations, the root mean square fluctuation (RMSF) of the first position uracil is 1.18 Å when base pairing to guanine (ASL^{Leu2}) compared to 0.72 Å (ASL^{Phe}) and 0.75 Å (ASL^{Ser}) when base pairing with an adenine. Thus, although A1493 interacts more favorably with a near-cognate guanine compared to a cognate adenine in the first position of the anticodon, the key interaction with the codon nucleotide is lost, resulting in a destabilization of the near-cognate codon−anticodon complex.

In contrast, the results of the simulations performed by Sanbonmatsu and Joseph (*20*) for mismatch in the first position show that a C-A mismatch in the first position results in the anticodon nucleotide losing its interaction with A1493. This is perhaps not surprising, since the only possibility for the codon cytosine and an (unprotonated) anticodon adenine to make any favorable interactions without steric clashes at the first position is displacement of the adenine into the major groove away from A1493. However, the different results for U-G and C-A mismatches at the first position could also be due to an incorrect modeling of the adenine in ref *20*, as experimental data for RNA have shown that the adenine in A-C mismatches is, in fact, protonated at N1 at neutral pH

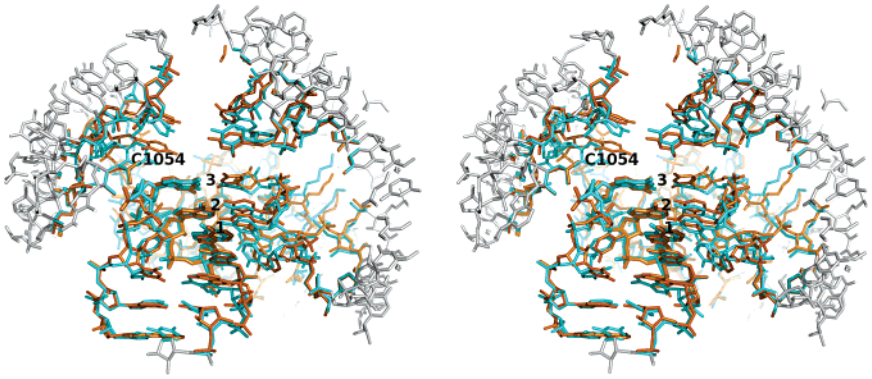

FIGURE 2: Stereoview of the structural agreement between the ASL^{Phe}-UUU simulation (orange) and crystal (blue and gray) structures. The orange- and blue-colored atoms are the atoms used in the RMSD calculation (all heavy atoms within 20 Å of the simulation center). The numbering refers to the first, second, and third positions in the codon−anticodon helix.

(*38*, *39*). Treating the adenine as protonated would most likely have given similar results to those observed here; i.e., the first position codon nucleotide would be displaced into the major groove.

The displacement of the codon uracil of the first position G-U wobble pair may also be compared to the results presented in a related study of base pair discrimination by the DNA polymerase β by Florián et al. (*40*), where it was observed that, in order to form a wobble base pair, the guanine of a G-T mismatch in the active site of the polymerase was displaced into the minor groove of the DNA helix. This is somewhat similar to the behavior observed here; however, A1493 sterically hinders the first position guanine to be displaced into the minor groove, instead forcing it to move toward the codon base, consequently displacing U1 into the major groove instead.

According to the crystal structures of Ogle et al. (*19*), A1492 does not span the minor groove when ASL^{Leu2} and a UUU codon are in the A-site, and accordingly this is how the ASL^{Leu2} simulations were carried out. However, in an attempt to discern the factors which cause A1492 not to span the minor groove in case of a first position mismatch, we conducted additional simulations of ASL^{Leu2} in which A1492 does span the minor groove. The results of these simulations show that the calculated binding free energies with A1492 spanning the minor groove are 1 kcal/mol more positive than when A1492 is not spanning the groove. Also, fluctuations (as measured by RMSF) of the first position uracil were larger when A1492 spanned the minor groove, indicating a less structurally stable complex (1.42 Å vs 1.18 Å for UUC and 1.72 Å vs 1.14 Å for UUU). The cause of the higher binding free energies is not readily discernible, but a plausible explanation is that A1492 would orient the codon to a position which causes unfavorable interactions between the first position uracil and its anticodon counterpart, if it spans the minor groove.

Discrimination at the Second Codon−Anticodon Base Pair. With cognate tRNA bound at the A-site, four hydrogen bonds involving A1492 which stabilize the interactions at the second position of the codon−anticodon helix are apparent from the simulations. These are between the 2′-hydroxyl of A1492 and the 2′-hydroxyl of the second codon nucleotide (U2), between the 2′-hydroxyl of U2 and the N3 of A1492, and between the hydrogens on N1 and N2 of G530 and the N1 of A1492 (Figure 4). In the case of the near-cognate ASLs (ASL^{Leu2} and ASL^{Ser}) A1492 does not span the minor groove (*19*) and thus does not have any of the interactions mentioned above.

It is thus clear that A1492 helps to stabilize cognate tRNAs at the second position of the codon−anticodon helix; however, it is not clear why A1492 does not span the minor groove in the near-cognate cases. In order to investigate this matter we also performed simulations of ASL^{Ser} with A1492 spanning the minor groove. For ASL^{Ser}, which has a G-U mismatch in the second position of the codon−anticodon helix, the interactions of A1492 with the codon−anticodon helix are disturbed, and A1492 is significantly destabilized. The RMSF of A1492 in the ASL^{Ser} simulation is 0.79 Å, compared to 0.57 Å in the ASL^{Leu2} and ASL^{Phe} simulations. The key interaction, which is lost in the case of ASL^{Ser}, is the hydrogen bond between the 2′-hydroxyl of the codon nucleotide and the N3 of A1492. This interaction serves to keep the codon nucleotide in a fixed position relative to A1492 (or vice versa). If the codon and the anticodon nucleotides are not complementary, the codon nucleotide will be forced into an orientation where it loses its interactions with A1492 in order to accommodate the hydrogen bonds to the anticodon nucleotide. We also find indication of preferential near-cognate ASL^{Ser} binding to the ribosome when A1492 is not in the groove. The calculated binding free energies for ASL^{Ser} to the near-cognate form of the ribosome (A1492 not spanning the minor groove) with UUC as codon are, for example, 0.6 kcal/mol more negative than the calculated values for ASL^{Ser} binding to the cognate form (A1492 spanning the minor groove). Thus, the simulations provide a reasonable explanation as to why A1492 does not span the minor groove when there is a mismatch at the first or second position.

It is also interesting to note that in our simulations with ASL^{Ser}, bound to either the UUU or UUC codons, the wobble geometry type of hydrogen bonding at the second position is present essentially throughout the trajectories. This is in contrast to the results of ref *20* where severe disruptions at both first and second positions were observed for the UCU-ASL^{Phe} mismatch. This discrepancy could again be due to not modeling adenine as protonated at N1 in ref *20*, which has been observed in experiments when adenine is base paired with cytosine (*38*, *39*).

Discrimination at the Third Codon−Anticodon Base Pair. A mismatch at the third, or wobble, position of the codon−anticodon helix is not as severe as a mismatch at the first or second position. This is easily understood by looking at a

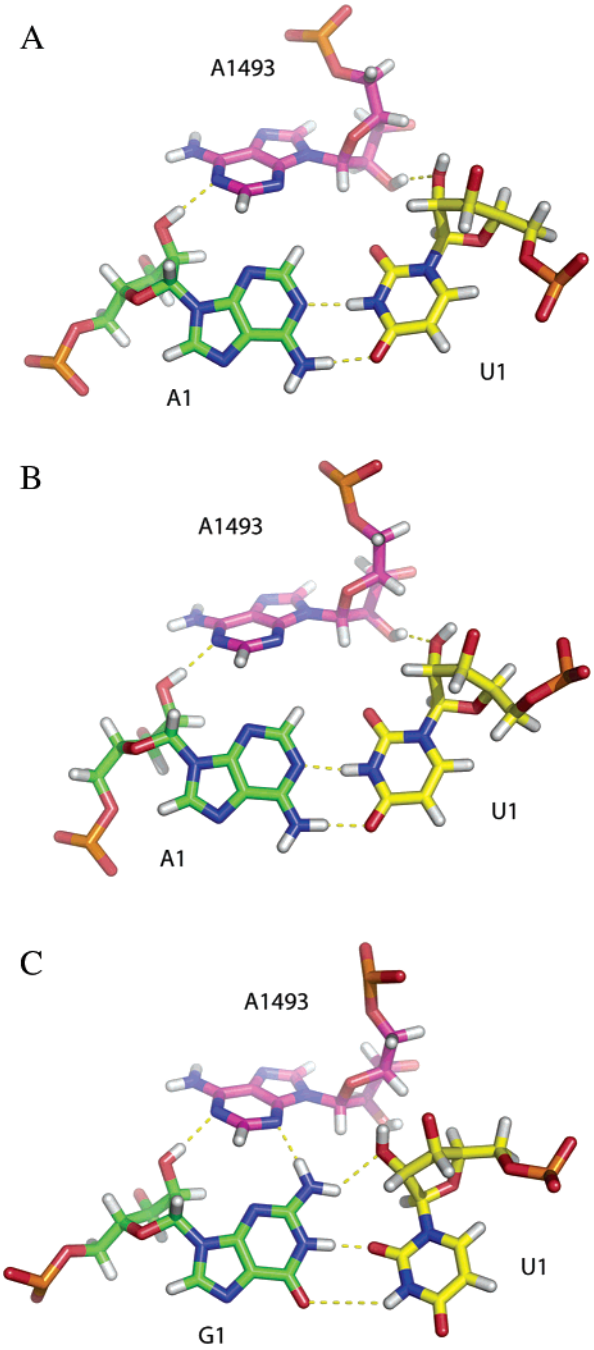

FIGURE 3: Representative average structures (50 ps) of residues involved in base pairing at the first (UUC) codon position with (A) AAG, (B) AGG, and (C) GAG anticodons in the A-site.

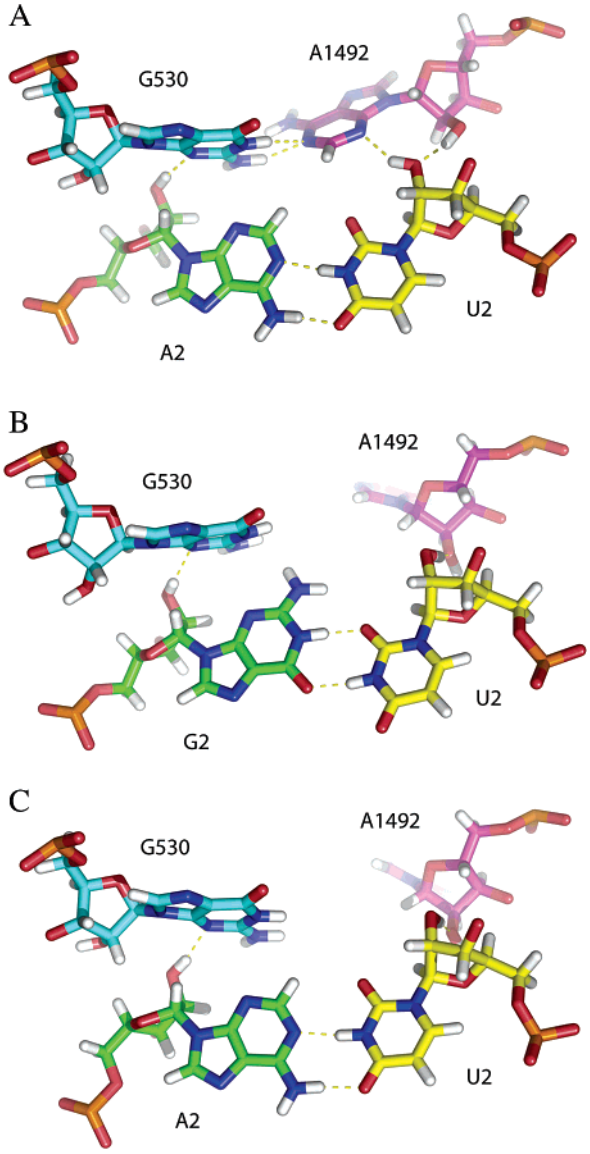

FIGURE 4: Representative average structures (50 ps) of the residues involved in base pairing at the second (UUC) codon position with (A) AAG, (B) AGG, and (C) GAG anticodons in the A-site.

codon table, where about half of all codons are translated into the same amino acid regardless of the nucleotide in the third position. Hence, the ribosome does not need to monitor this position as stringently as the first or second position, and the simulations do, in fact, show that the ribosome does not monitor base pairing at the third codon−anticodon position through direct interactions. The ribosome does however enhance the importance of a Watson−Crick base pair at the third position by preventing water from making hydrogen bonds to any unsatisfied donors/acceptors. As can be seen in Figure 5, G530 occludes solvent from the N2 of the anticodon G3, thus prohibiting hydrogen bonds otherwise present in the free state from forming and increasing the importance of a hydrogen bond acceptor in the codon. The distribution of hydrogen bond acceptors around the anticodon N2 hydrogen involved in hydrogen bonding with the codon nucleotide was calculated in terms of a radial distribution function (RDF) and shown in Figure 6. The plot clearly shows that this polar hydrogen is significantly desolvated in the mismatched base pair relative to both the matched base pair and water, contributing to the selective destabilization of the G-U wobble base pair at the third position.

Sanbonmatsu and Joseph (*20*) compared the structural dynamics of the UUU, UUA, and UUG codons interacting with the AAG (ASL^{Phe}) anticodon and found that, in the case of the UUA codon, the codon−anticodon interactions prevents A1492 from interacting with G530. They also find that the lack of interaction between A1492 and G530 exposes the third position to solvent. This observation may seem different from our finding that the third position is solvent shielded and, thus, enhances the importance of correct base pairing. However, their AAG-UUA complex has a more severe third position purine−purine (G-A) mismatch that causes a larger steric effect than our case with a G-U

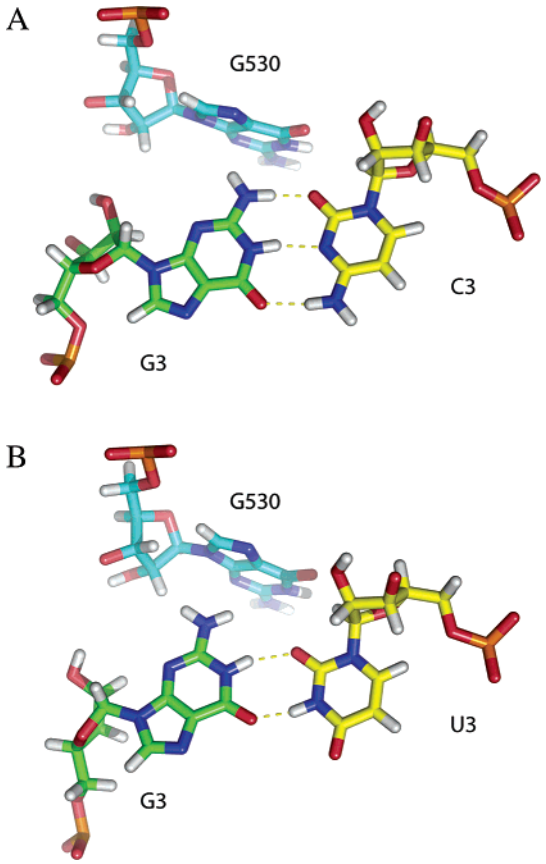

FIGURE 5: Representative average structures (50 ps) of the residues involved in base pairing at the third codon−anticodon position with cognate tRNA (AAG) in the A-site and (A) a nonwobble UUC or (B) wobble UUU mRNA.

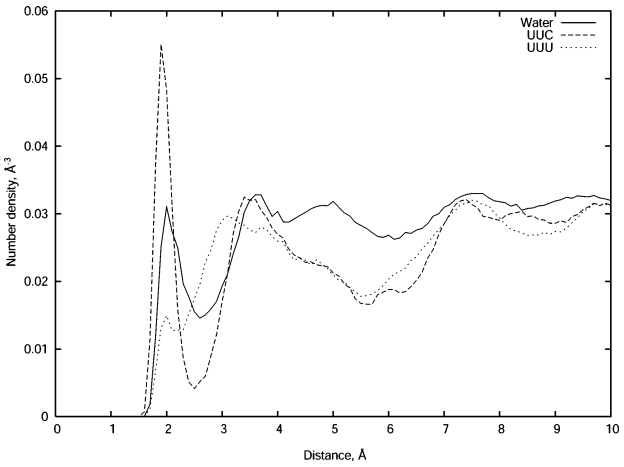

FIGURE 6: Radial distribution functions (RDFs) for one of the N2 hydrogens on the anticodon guanine in the third position to all hydrogen bond acceptors for the water, UUU (mismatch at third position), and UUC simulations.

mismatch. It is not mentioned in ref *20* whether the effect on A1492 was also obtained for the G-G mismatch (UUG codon), and this case was instead interpreted in terms of a reduced structural stability of the base pair compared to the UUU case. The authors also measured the solvent-accessible surface areas (SASA) of cognate (UUU) and near-cognate (UUA) codon−anticodon−rRNA complexes (G530, A1492, A1493 were included) and conclude that the SASA of near-cognate complexes is higher than for cognate complexes. The differences in the measured SASAs of 2033 Å^2 for UUU and 2080 Å^2 for UUA is, however, only slightly larger than the SASA of a methyl substituent and is thus probably only an effect of having a larger codon in the near-cognate case (adenine vs uracil). SASAs for the Phe anticodon in complex with UUU and UUC have also been reported by Lahiri and Nilsson (*41*), showing that the third position is actually more exposed with Watson−Crick than wobble geometry. Nevertheless, our simulations and those of ref *20*, which differ with respect to the type of mismatches, show that the differences in codon−anticodon stability at the third position may arise both from unsatisfied hydrogen bonding and steric effects.

Binding Free Energies. Average binding free energies were calculated for each codon−anticodon combination, utilizing the entire 1 ns production phase of the nine replicate simulations, by the LIE method (eq 1), and the results are shown in Table 1 and Figure 7. The calculated binding free energies are in very good agreement with experiment as judged by the root mean square (rms) and mean absolute errors of 0.55 and 0.50 kcal/mol, respectively. These calculations are the result of 6 × 9 × 1 ns = 54 ns of production phase MD simulation of the bound states and 3 × 9 × 1 ns = 27 ns of MD simulation of the free states for the entire data set. Such long simulation times would perhaps be prohibitive if the free energy of binding of many codon−anticodon interactions (there are 4096 possible combinations) is to be calculated. In order to discern if shorter simulation times were possible without sacrificing too much accuracy in the calculations of binding free energies, the production phase of the simulations was shortened to only 50 ps, yielding total production phase simulation times of 2.7 and 1.35 ns for bound and free states, respectively, for the entire data set. The ligand-surrounding energies and calculated binding free energies for this reduced computational scheme are shown in Table 2, and the rms error and mean absolute error are 0.53 and 0.45 kcal/mol, respectively. Hence, the obtained results are of similar quality, and we can therefore conclude that it is probably not necessary with nanosecond length simulations, but that shorter trajectories can be used as long as statistics from multiple simulations are collected.

From the above results, it is particularly noteworthy that the computational ranking of the mismatches is excellent with the wobble position mismatch giving about 1 kcal/mol destabilization compared to the cognate complex while a first or second position mismatch confers a destabilization of up to 3 kcal/mol. There has been no experimental binding affinities published for ASL^{Leu2} or ASL^{Ser} binding to the UUU codon, which encompasses a third position G-U mismatch in addition to the first or second position mismatches. Our results predict an additional decrease in binding affinity for these ASLs when introducing a third position wobble mismatch, as would be expected. The calculations also predict that two adjacent mismatches in the second and third position are more severe than if the first and third positions do not match.

The predominant energetic origin of discrimination is clearly the electrostatic component of the binding free energy. Compared to the cognate ASL^{Phe} complex with the UUC codon (AAG-UUC in Table 1), one finds that the relative electrostatic contributions for the AAG-UUU, GAG-UUC, GAG-UUU, AGG-UUC, and AGG-UUU combinations are 0.6, 2.4, 3.0, 1.9, and 3.7 kcal/mol less favorable, respec-

Table 1: Average Ligand-Surrounding Energies and Calculated Binding Free Energies for the Nine Replicate 1 ns Simulations[a]

anticodon−codon (3′−5′)-(5′−3′)	$\langle V_{l-s}^{vdW}\rangle_f$	$\langle V_{l-s}^{vdW}\rangle_b$	$\langle V_{l-s}^{el}\rangle_f$	$\langle V_{l-s}^{el}\rangle_b$	ΔG_{calc}	σ_M	ΔG_{obs}[c]
AAG-UUC	−46.9	−65.7	−144.3	−138.5	−7.5	0.46	−8.3
AAG-UUU	−46.9	−64.4	−144.3	−137.1	−6.7	0.47	−7.0
GAG-UUC	−46.9	−68.6	−170.1	−158.8	−5.7	0.83	−5.0
GAG-UUU	−46.9	−67.8	−170.1	−157.4	−5.0	0.87	N/A[b]
AGG-UUC	−46.4	−64.9	−174.3	−164.0	−5.5	0.60	−5.2
AGG-UUU	−46.4	−62.7	−174.3	−160.0	−3.4	0.51	N/A[b]

[a] All values are in kcal/mol. $\langle\ \rangle_f$ and $\langle\ \rangle_b$ denote the free and bound states of the ASL. σ_M is the standard error of the mean ΔG_{calc}. [b] No experimental data available. [c] Reference *19*.

tively. This can be compared to the total calculated relative binding free energies of 0.8, 1.8, 2.6, 2.0, and 4.1 kcal/mol for AAG-UUU, GAG-UUC, GAG-UUU, AGG-UUC, and AGG-UUU, respectively. That is, the electrostatic energy terms, which mainly reflect hydrogen-bonding interactions, apparently account for most of the stability differences.

In order to quantitatively address the question of whether the ribosome is able to enhance the intrinsic stability of codon−anticodon complexes in water, simulations were also performed on identical systems as above, except that the ribosomal parts were removed, i.e., mRNA complexed with tRNA in water. The results of these simulations are presented in Table 3. These results indicate that the ribosome additionally contributes about 1 kcal/mol to the discrimination between incorrect and correct codon−anticodon combinations. More specifically, the calculated binding free energies in water for the tRNA and mRNA anticodon−codon combinations [(3′−5′)−(5′−3′)] AAG-UUU, GAG-UUC, and AGG-UUC relative to AAG-UUC were found to be 0.0, 0.7, and 1.4 kcal/mol. Again, this should be compared to the calculated relative binding free energies for the same combinations in the ribosome: 0.8, 1.8, and 2.0 kcal/mol for AAG-UUU, GAG-UUC, and AGG-UUC relative to AAG-UUC. It is therefore very interesting to note that the calculations indeed show that the energetic discrimination between complexes is significantly enhanced by the ribosomal environment.

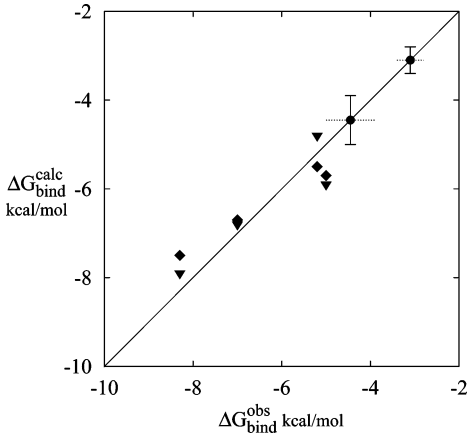

FIGURE 7: Calculated vs observed (*19*) binding free energies (kcal/mol) for four ASLs binding to the A-site of the 30S ribosomal subunit as calculated from 1 ns (diamonds) and 50 ps (triangles) of production phase molecular dynamics. Shown as circles are the predicted binding free energies of the two ASLs for which no experimental data were available. The error bars indicate the difference between the long and short simulations.

DISCUSSION

We have reported molecular dynamics simulations and binding free energy calculations that address the energetics of codon−anticodon recognition on the small ribosomal subunit. Simulations were carried out for the six different codon−anticodon combinations that result from considering three anticodon stem loops and two different codons. The structural agreement between average MD structures and existing crystallographic data is excellent, and the simulations support the proposed roles of key interactions involving the ribosomal groups A1492, A1493, and G530 in the codon−anticodon recognition process (*14*, *15*). Binding free energies were calculated using the linear interaction energy method, and the resulting affinities for different codon−anticodon combinations agree well with experimental data. The relatively large measured affinity ratios (*19*) between cognate and near-cognate complexes, on the order of 100, are thus reasonably well reproduced by the calculations. Furthermore, the calculations identify the polar contribution (mainly hydrogen bonding) as the main determinant of stability differences, as would be expected. Also, the results show that the ribosome indeed enhances the intrinsic stability differences compared to codon−anticodon (mRNA−tRNA) complexes in solution. This appears to be mainly achieved by the interactions involving the monitoring groups mentioned above and also by shielding of the triplets from solvent. In this respect, the proposal by Sanbonmatsu and Joseph (*20*) that the mRNA kink tests and amplifies the stability of base pairing in the first position is rather strange. That is, it is very difficult to see how solvent exposure could be used for amplification of energy differences. The idea that a near-cognate mismatch (ASL^{Phe}-CUC in this case) is thermodynamically more stable in a duplex than when adjacent to a kink (*20*) is also at variance with experimental facts (*3*, *11*, *13*, *42*). While structural fluctuations of such a mismatch may be lower in the interior of a duplex, the energetic penalty is still higher than if the mismatch is located at the end of a duplex or at a kink or a loop (*3*, *11*, *13*, *42*). This again underlines the fact that dynamic stability cannot directly be equated to thermodynamic stability.

The question of how closely the binding data for ASLs to the 30S decoding center A-site reflect the actual energetics of ternary complexes bound to the full ribosome is more difficult to address. However, the structural results obtained from X-ray crystallography and cryo-EM studies on whole ribosome complexes (*27*, *43*) support the relevance of the structural and energetic ASL data in that the tRNA anticodon evidently is positioned in the same manner. Recent data from Rodnina and co-workers (*44*) show a uniform response of

Table 2: Average Ligand-Surrounding Energies and Calculated Binding Free Energies for the Nine Replicate 50 ps Simulations[a]

anticodon−codon (3′−5′)-(5′−3′)	$\langle V_{l-s}^{vdW}\rangle_f$	$\langle V_{l-s}^{vdW}\rangle_b$	$\langle V_{l-s}^{el}\rangle_f$	$\langle V_{l-s}^{el}\rangle_b$	ΔG_{calc}	σ_M	ΔG_{obs}[c]
AAG-UUC	−46.8	−67.1	−142.8	−137.9	−7.9	0.72	−8.3
AAG-UUU	−46.8	−64.2	−142.8	−136.8	−6.8	0.73	−7.0
GAG-UUC	−46.2	−69.5	−169.4	−158.7	−5.9	0.78	−5.0
GAG-UUU	−46.2	−67.1	−169.4	−155.0	−3.9	1.26	N/A[b]
AGG-UUC	−46.5	−65.3	−172.6	−161.3	−4.8	0.93	−5.2
AGG-UUU	−46.5	−64.6	−172.6	−157.0	−2.8	1.09	N/A[b]

[a] All values are in kcal/mol. $\langle\ \rangle_f$ and $\langle\ \rangle_b$ denote the free and bound states of the ASL. σ_M is the standard error of the mean ΔG_{calc}. [b] No experimental data available. [c] Reference *19*.

Table 3: Average Ligand-Surrounding Energies and Calculated Binding Free Energies for Nine Replicate 1 ns Simulations of the ASL and mRNA Complex without the Ribosome[a]

anticodon−codon (3′−5′)-(5′−3′)	$\langle V_{l-s}^{vdW}\rangle_f$	$\langle V_{l-s}^{vdW}\rangle_b$	$\langle V_{l-s}^{el}\rangle_f$	$\langle V_{l-s}^{el}\rangle_b$	ΔG_{calc}	σ_M
AAG-UUC	−46.9	−60.2	−144.3	−145.8	−3.1	0.15
AAG-UUU	−46.9	−57.8	−144.3	−146.8	−3.0	0.05
GAG-UUC	−46.9	−61.6	−170.1	−169.4	−2.4	0.28
GAG-UUU	−46.9	−58.8	−170.1	−169.4	−1.8	0.06
AGG-UUC	−46.4	−59.2	−174.3	−172.8	−1.6	0.08
AGG-UUU	−46.4	−57.9	−174.3	−172.7	−1.4	0.23

[a] All values are in kcal/mol. $\langle\ \rangle_f$ and $\langle\ \rangle_b$ denote the free and bound states of the ASL. σ_M is the standard error of the mean ΔG_{calc}. Note that the constant γ in eq 1 is set to zero here, since these calculations represent the association of triplets in water.

about 4 kcal/mol more unfavorable binding for a set of mismatching codons interacting with $tRNA^{Phe}$. While these mismatches are of the A-C, G-A, and G-G type, i.e., different from those studied herein, one may get the impression that the relative energetics of tRNA (ternary complex) binding differs significantly from that of the ASLs. However, it is clear from experimental data on the stability of RNA duplexes that A-C, as well as G-A and G-G, mismatches are energetically more than 2 kcal/mol less favorable than G-U pairs (*42*), which may explain the apparent differences with respect to the ASL binding data (*19*). Regarding absolute binding affinities, one can also note that the cognate codon recognition is associated with a standard binding free energy of about −4 kcal/mol (*44*), while the sequence unspecific initial binding corresponds to about −8 kcal/mol (again at a 1 M standard state) (*16*). How these values relate to the binding free energy of −8.2 kcal/mol for ASL^{Phe} to the UUC codon (*15*) is not entirely clear, but a possible explanation would be that the difference between −12 (= −8 − 4) kcal/mol and the corresponding data for the ASL (−8.2 kcal/mol) indeed reflects the missing interactions in the latter system. An interesting question that also arises from a strong ($K_d \sim 1\ \mu M$) unspecific binding step is that it would appear to be a nonoptimal solution to the problem of discriminating against near-cognate tRNAs.

The relative effects of mismatches in the first or second position as compared to the third are thus reproduced, and the further destabilization of complexes harboring multiple mismatches is predicted by the calculations. Interestingly, these results predict that adjacent mismatches in the second and third positions are more severe (by 1.1−1.6 kcal/mol) than two mismatches flanking a Watson−Crick base pair at the second position, with the UUU codon. It may indeed seem logical that a matching base pair confers more stability to the complex if it is located at the center of a near-cognate triplet. This result is also precisely what emerges from the empirically derived thermodynamic base pairing additivity scheme of Turner and co-workers (*11*, *13*). It may not be warranted to generalize the above result for the ribosome since the detailed energetics may depend on the type of mismatches and, more generally, be sequence dependent. Nevertheless, for the UUU codon it is evident that first position mismatches, retaining U in the second position, all translate into similarly bulky hydrophobic amino acids according to the standard code. For second position mismatches with the Phe UUU codon the resulting errors (Ser, Tyr, Stop, Cys, Trp) are indeed more severe. This would thus be commensurable with the calculated binding energetics which predicts the latter type mismatch to be heavier penalized, suggesting that such features of the genetic code could have become fixed before proofreading emerged. The observation that the second codon position is generally more critical than the first in determining amino acid properties has been made before (see, e.g., ref *45*), but its possible origin in terms of simple binding thermodynamics has to our knowledge not been discussed.

It is also interesting to compare calculated and observed energetics of near-cognate ASL^{Leu2} binding to the UUU and UUC codons (Tables 1 and 2) to the overall accuracy in the initial selection for the very same codons recently measured by Bouakaz et al. (E. Bouakaz, M. Lovmar, M. Johansson, and M. Ehrenberg, personal communication). These measurements, which did not kinetically resolve the detailed steps on the initial selection pathway (codon recognition and GTP hydrolysis), yielded accuracy factors for ternary complex selection ($tRNA^{Phe}$ vs $tRNA^{Leu2}$) of 1150 and 510 for the UUU and UUC codons, respectively (Bouakaz et al., in preparation). Our average results (from Tables 1 and 2) for the stability ratios between ASL^{Phe} and ASL^{Leu2} to the two codons are 50 and 25, respectively. Hence, while the trend appears to be correct, it is clear that neither the calculated binding affinities nor the experimental data for ASL^{Phe} vs ASL^{Leu2} binding to UUC (*19*) can account for the entire accuracy in initial selection. In fact, Gromadski and Rodnina (*16*) have shown that for the case of $tRNA^{Phe}$ selection by cognate UUU and near-cognate CUC codons the GTPase

activation step is about 650-fold slower for the near-cognate case, demonstrating that GTPase activation contributes significantly to the initial selection. This effect is likely to be associated with a nonoptimal positioning or conformation of the GTPase center of the ternary complex that ultimately also should derive from mismatch at the decoding center. While the theoretical maximum accuracy factor of 10^4-10^5 (obtained by simply multiplying the differential codon−anticodon stabilities with the GTPase rates, both from ref *16*) that could be achieved in the initial selection from both codon binding and GTP hydrolysis is not fully utilized by the ribosome (*16*), it is clear that the higher off-rate (and thus dissociation constant) of near-cognate complexes is important for selection. Proofreading, on the other hand, contributes approximately an equal accuracy factor to that of the initial selection (*16*), and it seems likely that the higher rejection and lower peptidyl transfer rates of incorrect substrates also reflect positioning effects ultimately deriving from the codon−anticodon interactions.

In the deposited crystal structures for mismatch at the second and third codon−anticodon position [accession codes 1N33 and 1IBM, respectively (*15*, *19*)] the bases of the mismatch positions have geometries which are more consistent with Watson−Crick rather than wobble base-pairing geometry. This places the N3 of the codon uracil in close contact with the N1 of the anticodon guanine and the implied hydrogens extremely close to each other with resulting energetics very unfavorable. The authors acknowledge this and propose that either G or U exists in their unusual enol tautomers or that the model depicts an average of two distinct conformations. The notion of an enol tautomer in the second or third codon−anticodon position seems counter-intuitive for several reasons. First of all, this would retain Watson−Crick geometry at the mismatched position and prevent the ribosome (through A1492) from sensing a mismatch at the second position. The fact that the crystal structure with a mismatch at the second position does, in fact, indicate Watson−Crick geometry is most likely due to the presence of paromomycin, which displaces A1492 into the minor groove and forces the base pair to adopt Watson−Crick geometry through tautomerization. In the crystal structures of mismatch at the second position without paromomycin the mRNA and ASL are crystallographically disordered; hence there is no evidence for tautomerization of either base in the second position in the absence of paromomycin. Furthermore, since the enol forms of the nucleotides are about 4−5 kcal/mol less stable than the usual tautomers (*46*, *47*), the selective stabilization of the enol tautomer in the third position would in itself require interactions that are stronger than the ones discriminating between a match and a mismatch. Therefore, it seems most reasonable to model the interactions using the normal tautomers as done in this work. Since the calculated binding free energies for mismatch in the second or third position do in fact reproduce the observed binding free energies (*19*), we propose that in the absence of paromomycin the mismatched nucleotide binds as the normal keto tautomer in a wobble orientation.

It seems to us that the type of computational strategy employed here may be quite useful and interesting for further analysis of codon−anticodon recognition energetics. It is likely that the major determinant of the relative stabilities of cognate and noncognate complexes does reside in the interactions involving the triplets and their surrounding ribosomal groups. However, it may well be the case that the energetics of this recognition process is rather sequence specific so that mismatches are penalized differently depending on the sequence context. Possibly, the characterization of such patterns, both by experiments and by computations, could be related to the physicochemical nature of the resulting incorporated amino acids.

ACKNOWLEDGMENT

We thank Profs. Marina Rodnina and Måns Ehrenberg for useful discussions.

REFERENCES

1. Kurland, C. G., Hughes, D., and Ehrenberg, M. (1996) in *Escherichia coli and Salmonella typhimurium: Cellular and Molecular Biology* (Neidhart, F. C., Curtiss, R., III, Lin, E. C. C., Low, K. B., and Magasanik, B., Eds.) pp 979−1004, American Society for Microbiology Press, Washington, DC.
2. Meroueh, M., and Chow, C. S. (1999) Thermodynamics of RNA hairpins containing single internal mismatches, *Nucleic Acids Res. 27*, 1118−1125.
3. Sugimoto, N., Kierzek, R., Freier, S. M., and Turner, D. H. (1986) Energetics of internal GU mismatches in ribooligonucleotide helixes, *Biochemistry 25*, 5755−5759.
4. Kurland, C. G., Rigler, R., Ehrenberg, M., and Blomberg, C. (1975) Allosteric mechanism for codon-dependent tRNA selection on ribosomes, *Proc. Natl. Acad. Sci. U.S.A. 72*, 4248−4251.
5. Potapov, A. P. (1982) A stereospecific mechanism for the aminoacyl-tRNA selection at the ribosome, *FEBS Lett. 146*, 5−8.
6. Hopfield, J. J. (1974) Kinetic proofreading: a new mechanism for reducing errors in biosynthetic processes requiring high specificity, *Proc. Natl. Acad. Sci. U.S.A. 71*, 4135−4139.
7. Ninio, J. (1975) Kinetic amplification of enzyme discrimination, *Biochimie 57*, 587−595.
8. Thompson, R. C., and Stone, P. J. (1977) Proofreading of the codon-anticodon interaction on ribosomes, *Proc. Natl. Acad. Sci. U.S.A. 74*, 198−202.
9. Ruusala, T., Ehrenberg, M., and Kurland, C. G. (1982) Is there proofreading during polypeptide synthesis?, *EMBO J. 1*, 741−745.
10. Fourmy, D., Recht, M. I., Blanchard, S. C., and Puglisi, J. D. (1996) Structure of the A site of *Escherichia coli* 16S ribosomal RNA complexed with an aminoglycoside antibiotic, *Science 274*, 1367−1371.
11. Mathews, D. H., Sabina, J., Zuker, M., and Turner, D. H. (1999) Expanded sequence dependence of thermodynamic parameters improves prediction of RNA secondary structure, *J. Mol. Biol. 288*, 911−940.
12. Rodnina, M. V., and Wintermeyer, W. (2001) Fidelity of aminoacyl-tRNA selection on the ribosome: Kinetic and structural mechanisms, *Annu. Rev. Biochem. 70*, 415−435.
13. Xia, T. B., SantaLucia, J., Burkard, M. E., Kierzek, R., Schroeder, S. J., Jiao, X. Q., Cox, C., and Turner, D. H. (1998) Thermodynamic parameters for an expanded nearest-neighbor model for formation of RNA duplexes with Watson-Crick base pairs, *Biochemistry 37*, 14719−14735.
14. Carter, A. P., Clemons, W. M., Brodersen, D. E., Morgan-Warren, R. J., Wimberly, B. T., and Ramakrishnan, V. (2000) Functional insights from the structure of the 30S ribosomal subunit and its interactions with antibiotics, *Nature 407*, 340−348.
15. Ogle, J. M., Brodersen, D. E., Clemons, W. M., Tarry, M. J., Carter, A. P., and Ramakrishnan, V. (2001) Recognition of cognate transfer RNA by the 30S ribosomal subunit, *Science 292*, 897−902.
16. Gromadski, K. B., and Rodnina, M. V. (2004) Kinetic determinants of high-fidelity tRNA discrimination on the ribosome, *Mol. Cell 13*, 191−200.
17. Fahlman, R. P., Dale, T., and Uhlenbeck, O. C. (2004) Uniform binding of aminoacylated transfer RNAs to the ribosomal A and P sites, *Mol. Cell 16*, 799−805.
18. Olejniczak, M., and Uhlenbeck, O. C. (2006) tRNA residues that have coevolved with their anticodon to ensure uniform and accurate codon recognition, *Biochimie 88*, 943−950.

19. Ogle, J. M., Murphy, F. V., Tarry, M. J., and Ramakrishnan, V. (2002) Selection of tRNA by the ribosome requires a transition from an open to a closed form, *Cell 111*, 721−732.
20. Sanbonmatsu, K. Y., and Joseph, S. (2003) Understanding discrimination by the ribosome: Stability testing and groove measurement of codon-anticodon pairs, *J. Mol. Biol. 328*, 33−47.
21. Åqvist, J., Medina, C., and Samuelsson, J. E. (1994) New method for predicting binding-affinity in computer-aided drug design, *Protein Eng. 7*, 385−391.
22. Marelius, J., Kolmodin, K., Feierberg, I., and Åqvist, J. (1998) Q: A molecular dynamics program for free energy calculations and empirical valence bond simulations in biomolecular systems, *J. Mol. Graphics Modell. 16*, 213−225.
23. MacKerell, A. D., Wiorkiewiczkuczera, J., and Karplus, M. (1995) An all-atom empirical energy function for the simulation of nucleic-acids, *J. Am. Chem. Soc. 117*, 11946−11975.
24. Trobro, S., and Åqvist, J. (2005) Mechanism of peptide bond synthesis on the ribosome, *Proc. Natl. Acad. Sci. U.S.A. 102*, 12395−12400.
25. Trobro, S., and Åqvist, J. (2006) Analysis of predictions for the catalytic mechanism of ribosomal peptidyl transfer, *Biochemistry 45*, 7049−7056.
26. Shi, H. J., and Moore, P. B. (2000) The crystal structure of yeast phenylalanine tRNA at 1.93 Å resolution: A classic structure revisited, *RNA 6*, 1091−1105.
27. Yusupov, M. M., Yusupova, G. Z., Baucom, A., Lieberman, K., Earnest, T. N., Cate, J. H. D., and Noller, H. F. (2001) Crystal structure of the ribosome at 5.5 Å resolution, *Science 292*, 883−896.
28. Baker, N. A., Sept, D., Joseph, S., Holst, M. J., and McCammon, J. A. (2001) Electrostatics of nanosystems: Application to microtubules and the ribosome, *Proc. Natl. Acad. Sci. U.S.A. 98*, 10037−10041.
29. Ryckaert, J. P., Ciccotti, G., and Berendsen, H. J. C. (1977) Numerical integration of the cartesian equations of motion of a system with constraints: molecular dynamics of n-alkanes, *J. Comput. Phys. 23*, 327−341.
30. Lee, F. S., and Warshel, A. (1992) A local reaction field method for fast evaluation of long-range electrostatic interactions in molecular simulations, *J. Chem. Phys. 97*, 3100−3107.
31. Almlöf, M., Åqvist, J., Smalås, A. O., and Brandsdal, B. O. (2006) Probing the effect of point mutations at protein-protein interfaces with free energy calculations, *Biophys. J. 90*, 433−442.
32. Hansson, T., Marelius, J., and Åqvist, J. (1998) Ligand binding affinity prediction by linear interaction energy methods, *J. Comput.-Aided Mol. Des. 12*, 27−35.
33. Almlöf, M., Brandsdal, B. O., and Åqvist, J. (2004) Binding affinity prediction with different force fields: Examination of the linear interaction energy method, *J. Comput. Chem. 25*, 1242−1254.
34. Stahl, G., McCarty, G. P., and Farabaugh, P. J. (2002) Ribosome structure: revisiting the connection between translational accuracy and unconventional decoding, *Trends Biochem. Sci. 27*, 178−183.
35. Ogle, J. M., and Ramakrishnan, V. (2005) Structural insights into translational fidelity, *Annu. Rev. Biochem. 74*, 129−177.
36. Doherty, E. A., Batey, R. T., Masquida, B., and Doudna, J. A. (2001) A universal mode of helix packing in RNA, *Nat. Struct. Biol. 8*, 339−343.
37. Nissen, P., Ippolito, J. A., Ban, N., Moore, P. B., and Steitz, T. A. (2001) RNA tertiary interactions in the large ribosomal subunit: The A-minor motif, *Proc. Natl. Acad. Sci. U.S.A. 98*, 4899−4903.
38. Pan, B. C., Mitra, S. N., and Sundaralingam, M. (1998) Structure of a 16-mer RNA duplex r(GCAGACUUAAAUCUGC)(2) with wobble C·A(+) mismatches, *J. Mol. Biol. 283*, 977−984.
39. Jang, S. B., Hung, L. W., Chi, Y. I., Holbrook, E. L., Carter, R. J., and Holbrook, S. R. (1998) Structure of an RNA internal loop consisting of tandem C-A(+) base pairs, *Biochemistry 37*, 11726−11731.
40. Florian, J., Goodman, M. F., and Warshel, A. (2002) Theoretical investigation of the binding free energies and key substrate-recognition components of the replication fidelity of human DNA polymerase beta, *J. Phys. Chem. B 106*, 5739−5753.
41. Lahiri, A., and Nilsson, L. (2000) Molecular dynamics of the anticodon domain of yeast tRNA(Phe): Codon-anticodon interaction, *Biophys. J. 79*, 2276−2289.
42. Kierzek, R., Burkard, M. E., and Turner, D. H. (1999) Thermodynamics of single mismatches in RNA duplexes, *Biochemistry 38*, 14214−14223.
43. Valle, M., Zavialov, A., Li, W., Stagg, S. M., Sengupta, J., Nielsen, R. C., Nissen, P., Harvey, S. C., Ehrenberg, M., and Frank, J. (2003) Incorporation of aminoacyl-tRNA into the ribosome as seen by cryo-electron microscopy, *Nat. Struct. Biol. 10*, 899−906.
44. Gromadski, K. B., Daviter, T., and Rodnina, M. V. (2006) A uniform response to mismatches in codon-anticodon complexes ensures ribosomal fidelity, *Mol. Cell 21*, 369−377.
45. Crick, F. H. (1968) The origin of the genetic code, *J. Mol. Biol. 38*, 367−379.
46. Colominas, C., Luque, F. J., and Orozco, M. (1996) Tautomerism and protonation of guanine and cytosine. Implications in the formation of hydrogen-bonded complexes, *J. Am. Chem. Soc. 118*, 6811−6821.
47. Hanus, M., Ryjacek, F., Kabelac, M., Kubar, T., Bogdan, T. V., Trygubenko, S. A., and Hobza, P. (2003) Correlated ab initio study of nucleic acid bases and their tautomers in the gas phase, in a microhydrated environment and in aqueous solution. Guanine: Surprising stabilization of rare tautomers in aqueous solution, *J. Am. Chem. Soc. 125*, 7678−7688.

BI061713I